

# Scalable Algorithms for High Order Approximations on Compact Stencils

Yury Gryazin<sup>1</sup>, Ronald Gonzales, Yun Teck Lee

Idaho State University, Department of Mathematics and Statistics, 921 S. 8th Ave., Stop 8085, Pocatello, ID 83209, USA

## Abstract

The recent development of parallel technologies on modern desktop computers makes parallelization of the proposed numerical approaches a priority in algorithmic research. The main performance improvement in the upcoming years will be made based on the increasing number of cores on modern CPUs. This shifts the focus of the algorithmic research from the development of the sequential numerical methods to the parallel methodology. In this paper, we present an efficient parallel direct algorithm for the compact high-order approximation of the 3D Helmholtz equation. The developed method is based on a combination of the separation of variables technique and a Fast Fourier Transform (FFT) type method. The results of the implementation of this method in OpenMP, MPI and Hybrid programming environments on the multicore computers and multiple node clusters are presented. We considered a generalization of the presented algorithm to the solution of linear systems obtained from approximation on the compact 27-point 3D stencils on the rectangular grids with similar stencil coefficients. As an example of the diversity of applications, the direct parallel implementation of a compact fourth-order approximation scheme for a convection-diffusion equation is considered. The developed parallel algorithms present efficient direct solvers for many important applications, but they can be used as highly efficient preconditioners for a variety of iterative numerical methods in more general settings. In many situations, the efficiency of the iterative algorithms is determined by the robustness of the preconditioning technique, the presented methods have a wide range of applications. In this paper, we demonstrate the scalability of the developed numerical algorithms on a series of representative test problems.

*Keywords:* Compact finite-difference schemes, FFT, parallel algorithms, OpenMP, MPI, Hybrid

## 1. Introduction

In recent years, the problem of increasing the resolution of existing numerical solvers has become an urgent task in many areas of science and engineering. Most of the existing efficient solvers for structured matrices were developed for lower order approximations of partial differential equations. The need for improved accuracy of the underlying algorithms leads to modified linear systems. As a result, the numerical solvers must be modified (see e.g. [1]). The time and memory constraints of practical applications make utilization of the existing sequential methods unacceptable in many situations. The development of the parallel algorithms for the implementation of the new high-resolution schemes becomes the necessary stage in the simulation process of many natural phenomena and engineering applications.

The focus of this paper is to introduce an efficient parallel direct solver for the recently developed high-order approximation compact schemes for 3D Helmholtz equation (see e.g. [2, 3]) in both shared and distributed memory programming environments. We extend the developed parallel technique to solve more general linear systems obtained from approximations on 3D compact 27 point stencils with similar constraints on the stencil coefficients. The goal is to demonstrate efficiency

and scalability of the proposed direct parallel algorithms for the solution of the compact high-order approximation finite-difference schemes.

First, we focus on the description of the compact second, fourth and sixth order approximation FFT-type direct solvers for the three-dimensional Helmholtz equation with nonconstant coefficient depending on one spacial variable,  $z$ . This algorithm can be used in many important applications as a stand-alone parallel solver, but it can be used as a preconditioner in the more general three dimensional Helmholtz equation with non-constant coefficient depending on three spacial variables and nonreflecting boundary conditions ([2], [3]).

The model problem considered in the paper is the numerical solution of

$$\nabla^2 u + k^2 u = f, \quad \text{in } \Omega, \quad (1)$$

where  $\Omega = \{(x, y, z) \in \mathbb{R}^3 | L_x^l \leq x \leq L_x^r, L_y^l \leq y \leq L_y^r, L_z^l \leq z \leq L_z^r\}$ ,  $L_x^l < L_x^r, L_y^l < L_y^r, L_z^l < L_z^r$  and  $k$  is a complex valued coefficient depending only on  $z$ . The boundary conditions

$$u = 0, \quad \text{on } \partial\Omega_1 = \{(x, y, z) \in \Omega | x = L_x^l, L_x^r \text{ or } y = L_y^l, L_y^r\}, \quad (2)$$
$$\alpha_z \frac{\partial u}{\partial z} + \beta_z u = g(x, y), \quad \text{on } \partial\Omega_2 = \{(x, y, z) \in \Omega | z = L_z^l, L_z^r\},$$

where  $\alpha_z, \beta_z \in \mathbb{C}$ . These algorithms can be easily extended to the Neumann boundary conditions on the sides of the computational domain instead of the Dirichlet boundary conditions considered in this paper (see e.g. [4], [5])

<sup>1</sup>Corresponding author, Email: gryazin@isu.edu

The resulting discretization leads to a system of linear equations with block 27-diagonal structure. In general, the matrix of this system is neither positive definite nor Hermitian. If an efficient direct solver can be applied then it is a natural choice. In this case, the dependency of the coefficient on only the  $z$  variable allows the use of the separation of variable technique based on FFT for an efficient direct solution of the discretized system. The well-known FFTW package ([6]) for the standard implementation of the discrete sine transform (DST) in the horizontal  $xy$ -plane based on the FFT algorithm is utilized. This direct solver requires  $O(N_x N_y N_z \log N)$  operations, where  $N = \max(N_x, N_y)$  and  $N_x, N_y$ , and  $N_z$  are the numbers of grid points in  $x, y$ , and  $z$  directions respectively.

The advantage of this approach is the natural parallelization of the proposed compact schemes on the DST and inverse DST steps. The transform implementation allows parallelization into the subdomains separated by the horizontal  $xy$ -plane. On the step of the solution of the tridiagonal independent linear systems, parallelization is implemented by the division of computational domain into a sequence of subdomains by the series of vertical  $xz$ - and  $yz$ -planes. In the distributed memory environment such as MPI, the communication between the processes is required only between the transforms and independent solver stages.

Numerical experiments with test problems demonstrate the high efficiency of the parallel implementation of the second, fourth and sixth order compact finite-difference schemes. The performance of the developed methods is compared to the parallel implementation of the multigrid algorithm on the multi-node cluster presented in ([7]). The parallel algorithms presented here significantly outperformed the mentioned iterative method in both memory usage and "wall time" measure.

The remainder of the paper is organized as follows. In Section 2 the description of the second, fourth and sixth order approximation compact schemes are presented. Section 3 focuses on the generalization of the developed parallel algorithm to the general compact stencil calculations with required properties. Section 4 presents the details of the OpenMP, MPI and Hybrid implementation of the developed algorithms. In Section 5, the effectiveness of the proposed parallel algorithms is demonstrated on a series of test problems.

## 2. Compact Discretizations

To introduce high order approximation compact schemes for the solution of the three-dimensional Helmholtz equation (1) with the boundary conditions (2) we consider a grid  $\Omega_h = \{(x_i, y_j, z_l) \mid x_i = L_x^l + ih_x, y_j = L_y^l + jh_y, z_l = L_z^l + lh_z, i = 1, \dots, N_x, j = 1, \dots, N_y, l = 1, \dots, N_z\}$ , where  $h_\alpha = (L_\alpha^r - L_\alpha^l)/(N_\alpha + 1)$ ,  $\alpha = x, y, z$  are grid steps in  $\alpha$  direction. The standard notation for the first and second order central differences at  $(i, j, l)$ -th grid point is given by

$$\delta_x u_{i,j,l} = \frac{u_{i+1,j,l} - u_{i-1,j,l}}{2h_x}, \quad \delta_x^2 u_{i,j,l} = \frac{u_{i-1,j,l} - 2u_{i,j,l} + u_{i+1,j,l}}{h_x^2},$$

where  $u_{i,j,l} = u(x_i, y_j, z_l)$ . The difference operators  $\delta_y, \delta_z, \delta_y^2$  and  $\delta_z^2$  used in the following sections are defined similarly. The second order approximation scheme can be written as

$$\left(\delta_x^2 + \delta_y^2 + \delta_z^2\right) U_{i,j,l} + k_l^2 U_{i,j,l} = f_{i,j,l} \quad (3)$$

where  $k_l = k(z_l)$  and  $U_{i,j,l}$  is the second order finite-difference approximation to the solution  $u_{i,j,l}$  of (1, 2).

### 2.1. Fourth order Padé approximation compact scheme

Now, we consider the standard fourth order Padé finite difference compact approximation (see e.g. [8]) of (1). The fourth order rational approximation of a second derivative can be presented in the form

$$\frac{\partial^2 u}{\partial \alpha^2} \Big|_{i,j,l} = \left(1 + \frac{h_\alpha^2}{12} \delta_\alpha^2\right)^{-1} \delta_\alpha^2 u_{i,j,l} + O(h_\alpha^4), \quad \alpha = x, y, z.$$

By substituting this approximation into (1), we obtain

$$\begin{aligned} & \left(1 + \frac{h_x^2}{12} \delta_x^2\right)^{-1} \delta_x^2 u_{i,j,l} + \left(1 + \frac{h_y^2}{12} \delta_y^2\right)^{-1} \delta_y^2 u_{i,j,l} + \\ & \left(1 + \frac{h_z^2}{12} \delta_z^2\right)^{-1} \delta_z^2 u_{i,j,l} + k_l^2 u_{i,j,l} = f_{i,j,l} + O\left(\max(h_x^4, h_y^4, h_z^4)\right), \end{aligned}$$

which gives

$$\begin{aligned} & \left(\delta_x^2 + \delta_y^2 + \delta_z^2\right) U_{i,j,l} + \frac{(h_x^2 + h_y^2)}{12} \delta_x^2 \delta_y^2 U_{i,j,l} + \frac{(h_x^2 + h_z^2)}{12} \delta_x^2 \delta_z^2 U_{i,j,l} \\ & + \frac{(h_y^2 + h_z^2)}{12} \delta_y^2 \delta_z^2 U_{i,j,l} + \left(1 + \frac{h_x^2}{12} \delta_x^2 + \frac{h_y^2}{12} \delta_y^2 + \frac{h_z^2}{12} \delta_z^2\right) (k_l^2 U_{i,j,l}) \\ & = \left(1 + \frac{h_x^2}{12} \delta_x^2 + \frac{h_y^2}{12} \delta_y^2 + \frac{h_z^2}{12} \delta_z^2\right) f_{i,j,l} = f_{i,j,l}^{(IV)} \end{aligned} \quad (4)$$

where  $U_{i,j,l}$  is the fourth order compact finite-difference approximation to  $u_{i,j,l}$ .

#### 2.1.1. Sixth order approximation compact scheme

In this section we present a three-dimensional compact sixth order approximation finite-difference scheme. The scheme requires a uniform grid step so we assume  $h = h_x = h_y = h_z$ . Using the appropriate derivatives of (1) we can write the sixth order compact approximation of the equation in the form

$$\begin{aligned} & \left(\delta_x^2 + \delta_y^2 + \delta_z^2\right) \left(1 + \frac{k_l^2 h^2}{30}\right) U_{i,j,l} + \frac{h^4}{30} \delta_x^2 \delta_y^2 \delta_z^2 U_{i,j,l} + k_l^2 U_{i,j,l} + \\ & \frac{h^2}{6} (\delta_x^2 \delta_y^2 + \delta_x^2 \delta_z^2 + \delta_y^2 \delta_z^2) \left(1 + \frac{k_l^2 h^2}{15}\right) U_{i,j,l} + \frac{h^2}{20} \Delta_h (k_l^2 U_{i,j,l}) = \\ & f_{i,j,l} + \frac{h^2}{12} \nabla^2 f_{i,j,l} + \frac{h^4}{360} \nabla^4 f_{i,j,l} + \\ & \frac{h^4}{90} \left(\frac{\partial^4 f}{\partial x^2 \partial y^2} + \frac{\partial^4 f}{\partial x^2 \partial z^2} + \frac{\partial^4 f}{\partial y^2 \partial z^2}\right)_{i,j,l} = f_{i,j,l}^{(VI)}, \end{aligned} \quad (5)$$

where

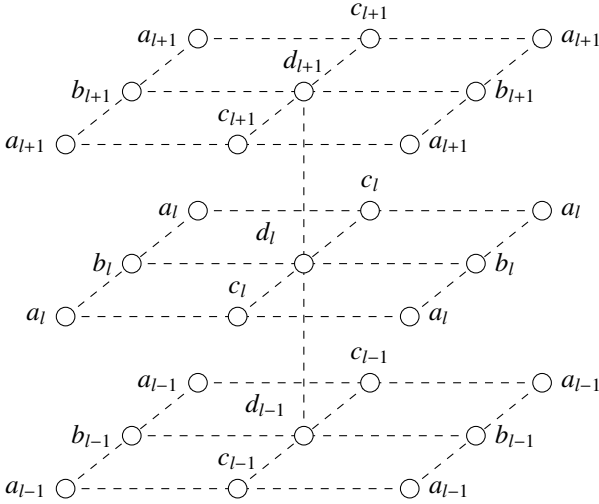
$$\Delta_h (k_l^2 U_{i,j,l}) = k_l^2 U_{i,j,l} + \left( \frac{\partial^2}{\partial z^2} (k^2) - k^4 \right)_l + 2[(k^2)_z]_l \left[ \delta_z \left( 1 + \frac{h^2}{6} (\delta_x^2 + \delta_y^2 + k_l^2) \right) U_{i,j,l} - \frac{h^2}{6} (f_z)_{i,j,l} \right].$$

This compact scheme was developed in [7] for the approximation of the three-dimensional Helmholtz equation with non-constant coefficient and Dirichlet boundary conditions. The compact sixth order approximation of the Sommerfeld-like boundary conditions was developed in our previous publication ([2]). The partial derivatives of  $f(x, y, z)$  in (5) are approximated by using the implicit compact approximation technique described in ([8]). It requires boundary conditions on the corresponding derivatives. In many important applications, we can impose zero boundary conditions on these derivatives.

### 3. Scalable FFT Compact Direct Solver

This section presents a generalization of parallel direct solvers for the second, fourth and sixth order compact schemes presented in Section 2. Here we consider the generalized 27-diagonal linear system satisfying a set of required conditions. Figure 1 demonstrates the 3D compact stencil form corresponding to this system.

Figure 1: 27-Point Stencil



#### 3.1. Stencil Form of the Schemes

All three compact schemes under consideration can be written in this stencil form. Also, this generalized type of numerical schemes can be expressed at every grid point  $(i, j, l)$  as

$$\sum_{v=l-1}^{v=l+1} \left( a_v [U_{i-1,j-1,v} + U_{i-1,j+1,v} + U_{i+1,j-1,v} + U_{i+1,j+1,v}] + b_v [U_{i-1,j,v} + U_{i+1,j-1,v}] + c_v [U_{i,j-1,v} + U_{i,j+1,v}] + d_v U_{i,j,v} \right) = F_{i,j,l}. \quad (6)$$

This equation corresponds to the  $(i + N_x \cdot j + N_x \cdot N_y \cdot l)$ -th row in the resulting linear system  $AU = F$ . The following subsections specifies the stencil coefficients in all three compact schemes under consideration.

#### 3.2. Second Order

Let  $R_{zx} = h_z^2/h_x^2$  and  $R_{zy} = h_z^2/h_y^2$ . In the second order scheme, there are only five nonzero parameters

$$b_l = R_{zx}, c_l = R_{zy}, d_{l-1} = d_{l+1} = 1, d_l = -2(R_{zx} + R_{zy} + 1) + h_z^2 k_l^2.$$

The right hand side is given by  $F_{i,j,l} = h_z^2 f_{i,j,l}$ .

#### 3.3. Fourth Order

The nonzero coefficients in the fourth order scheme are

$$\begin{aligned} b_{l-1} &= b_{l+1} = (1 + Rz_x)/12, & c_{l-1} &= c_{l+1} = (1 + Rz_y)/12, \\ d_{l-1} &= 2/3 - (Rz_x + Rz_y)/6 + h_z^2 k_{l-1}^2/12, \\ d_{l+1} &= 2/3 - (Rz_x + Rz_y)/6 + h_z^2 k_{l+1}^2/12, \\ a_l &= (Rz_x + Rz_y)/12, & b_l &= (4Rz_x - Rz_y - 1 + h_z^2 k_l^2/2)/6, \\ c_l &= (4Rz_y - Rz_x - 1 + h_z^2 k_l^2/2)/6, \\ d_l &= -4(1 + Rz_x + Rz_y)/3 + h_z^2 k_l^2/2. \end{aligned}$$

Then the fourth order right hand side is given by  $F_{i,j,l} = h_z^4 f_{i,j,l}^{IV}$ .

#### 3.4. Sixth Order

In the case of the sixth order scheme (5), the grid step size  $h$  is uniform in all three direction. The scheme parameters are calculated as

$$\begin{aligned} a_{l-1} &= a_{l+1} = 1/30, \\ b_{l-1} &= c_{l-1} = 1/10 + h^2 k_{l-1}^2/90 - h^3 k_{z,l}^2/120, \\ b_{l+1} &= c_{l+1} = 1/10 + h^2 k_{l+1}^2/90 + h^3 k_{z,l}^2/120, \\ d_{l-1} &= 7/15 - h^2 k_{l-1}^2/90 - (h^3 k_{z,l}^2/20)(1/3 + h^2 k_{l-1}^2/6), \\ d_{l+1} &= 7/15 - h^2 k_{l+1}^2/90 + (h^3 k_{z,l}^2/20)(1/3 + h^2 k_{l+1}^2/6), \\ a_l &= 1/10 + h^2 k_l^2/90, & b_l &= c_l = 7/15 - h^2 k_l^2/90, \\ d_l &= -64/15 + 14h^2 k_l^2/15 - h^4 (k_l^2)^2/20 + h^4 k_{z,l}^2/20. \end{aligned}$$

The right hand side is given by  $F_{i,j,l} = h_z^6 f_{i,j,l}^{VI}$ .

#### 3.5. Forth Order Approximation Scheme for 3D Convection-Diffusion Equation

In this subsection, the versatility of the proposed parallel solver is illustrated on the 3D convection-diffusion equation with dominant convection in the  $z$ -direction. The steady-state 3D convection-diffusion equation can be written as

$$\nabla^2 u + \alpha \frac{\partial u}{\partial x} + \beta \frac{\partial u}{\partial y} + \gamma \frac{\partial u}{\partial z} = g(x, y, z), \quad (7)$$

where  $\alpha$ ,  $\beta$  and  $\gamma$  are variable or constant convection coefficients in the  $x$ -,  $y$ - and  $z$ -directions respectively and  $f$  is a

forcing function. We assume that the horizontal gradient is significantly smaller than the first derivative of  $u$  in the  $z$ -direction. This is a common situation in the modeling of atmospheric heat convection. Then the equation (7) becomes

$$\nabla^2 u + \gamma \frac{\partial u}{\partial z} = g(x, y, z), \quad (8)$$

We extend the work done in ([9]) on the 2D convection diffusion equation to the 3D case. Using the relevant derivatives of the original equation (7), the compact fourth order approximation scheme can be presented in the form similar to (4) with the following nonzero stencil coefficients

$$\begin{aligned} b_{l\pm 1} &= (1 + Rz_x)(2 \pm \gamma h_z)/24, \quad c_{l\pm 1} = (1 + Rz_y)(2 \pm \gamma h_z)/24, \\ d_{l\pm 1} &= 2/3 - (Rz_x + Rz_y)/6 \pm \frac{h_z \gamma}{12} (4 - Rz_x - Rz_y \pm h_z \gamma), \\ a_l &= (Rz_x + Rz_y)/12, \quad b_l = (4Rz_x - Rz_y - 1)/6, \\ c_l &= (4Rz_y - Rz_x - 1)/6, \quad d_l = -4(1 + Rz_x + Rz_y)/3 - h_z^2 \gamma^2/6. \end{aligned}$$

Then the right hand side of the resulting linear system can be presented as

$$F_{i,j,l} = h_z^2 \left[ g + \frac{h_x^2}{12} \frac{\partial^2 g}{\partial x^2} + \frac{h_y^2}{12} \frac{\partial^2 g}{\partial y^2} + \frac{h_z^2}{12} \left( \gamma \frac{\partial g}{\partial z} + \frac{\partial^2 g}{\partial z^2} \right) \right]_{i,j,k} \quad (9)$$

For simplicity, the right hand side of (7) is assumed to be twice continuously differentiable. The resulting matrix could be used in a more general setting as an excellent preconditioner in an iterative method. The efficiency of such a preconditioner, the authors will address in our following publications. In this paper, the focus is on the direct parallel solution of the resulting compact scheme.

### 3.6. FFT Solver for Compact Stencil

The following derivation presents an efficient way to parallelization of the proposed direct solver applied to the resulting linear system. The numerical scheme (6) can be presented in block three diagonal form and can be written as

$$\begin{aligned} C_l U_l + C_{p,l} U_2 &= F_l, \\ C_{m,l} U_{l-1} + C_l U_l + C_{p,l} U_{l+1} &= F_l, \quad l = 2, N_z - 1, \\ C_{m,N_z} U_{N_z-1} + C_{N_z} U_{N_z} &= F_{N_z}. \end{aligned}$$

Here, the vectors  $U_l$  and  $F_l$  are the parts of the unknown vector  $U$  and the right hand side  $F$  with  $l = 1, \dots, N_z$ . The nine diagonal matrices  $C_{m,l}$ ,  $C_l$ , and  $C_{p,l}$  are defined by the coefficients in (6). These matrices can be simultaneously diagonalized by using the  $N_x \cdot N_y \times N_x \cdot N_y$  orthogonal matrix of eigenvectors  $V$  defined by

$$V_{i,j}^{n,m} = \frac{2}{\sqrt{(N_x + 1)(N_y + 1)}} \sin\left(\frac{\pi n i}{N_x + 1}\right) \sin\left(\frac{\pi m j}{N_y + 1}\right),$$

where  $1 \leq i, n \leq N_x$  and  $1 \leq j, m \leq N_y$ . The corresponding eigenvalues  $\lambda_{i,j,\nu}$  for the matrices  $C_{m,l}$ ,  $C_l$ , and  $C_{p,l}$  are given by

$$\begin{aligned} \lambda_{i,j,\nu} &= 4a_\nu \cos\left(\frac{(i+1)\pi}{N_x+1}\right) \cos\left(\frac{(j+1)\pi}{N_y+1}\right) + \\ &2b_\nu \cos\left(\frac{(i+1)\pi}{N_x+1}\right) + 2c_\nu \cos\left(\frac{(j+1)\pi}{N_y+1}\right) + d_\nu, \\ 0 &\leq i < N_x, \quad 0 \leq j < N_y, \quad \nu = l-1, l, l+1. \end{aligned}$$

Since the matrices  $\Lambda_m = V^T C_m V$ ,  $\Lambda = V^T C V$  and  $\Lambda_p = V^T C_p V$  are the diagonal matrices of eigenvalues, the original system can be presented as a set of  $N_x \cdot N_y$  independent linear systems of size  $N_z$  by  $N_z$  in the following manner

$$\begin{aligned} C_m U_{l-1} + C U_l + C_p U_{l+1} &= F_l \\ V^T C_m V V^T U_{l-1} + V^T C V V^T U_l + V^T C_p V V^T U_{l+1} &= V^T F_l \\ \Lambda_m W_{l-1} + \Lambda W_l + \Lambda_p W_{l+1} &= \bar{F}_l \end{aligned}$$

where  $W_l = V^T U_l$  and  $\bar{F}_l = V^T F_l$ .

Each independent system in the set is tridiagonal and can be efficiently solved using LU decomposition with  $O(N_z)$  computational complexity. The solutions of each system in the set is independent of each other. Therefore, it can be efficiently parallelized on multicore CPUs and clusters.

Prior to solving these independent systems, the transformed right-hand side vectors  $\bar{F}_l = V^T F_l$ ,  $l = 1, \dots, N_z$  must be found. The matrix-vector multiplication in this calculation can be seen as a 2D discrete sine transform (DST) of the right-hand side vector  $F_l$ . This transform can be found by using the FFT algorithm with computational complexity  $O(N_x \cdot N_y \ln(N_x \cdot N_y))$ . In our solver, the standard implementation of FFT from the open source C library developed at Massachusetts Institute of Technology, namely FFTW [6] was used.

## 4. Parallelization

In this section, the details of the OpenMP, MPI and Hybrid implementation of the developed direct solvers are considered. We discuss the limitation and advantages of each implementation depending on particular computer architecture. The goal is to demonstrate the scalability of the developed methods on modern multicore desktops and multi-node clusters.

### 4.1. OpenMP

First, we consider the parallelization of the direct solver using OpenMP programming interface. OpenMP makes use of shared memory architecture and thus allows every thread to access all allocated memory in the program. Usually, it allows a significant reduction in communication time between different threads. While this is a powerful parallelization tool it is very restrictive. OpenMP programs can only run on a single computer with shared memory. On a large multi-node cluster, this typically restricts the parallel execution to a single node with the typical number of cores available for parallelization about 16 - 32. However, the more significant limitation is the required random access memory (RAM) allocation. In many situations, the computations with the desired modeling parameters require the vast amounts of RAM simply unavailable on a single machine.

Despite its limitations, the shared address model allows a relatively simple implementation and excellent speed up in the execution of structured blocks. Algorithm 1 shows how OpenMP was used to implement the developed parallel direct solver.

---

**Algorithm 1** OpenMP 3D Helmholtz Direct Solver

---

```
1: #pragma omp parallel for
2: for  $l = 1, \dots, N_z$  do
3:   2D forward DST in  $x-, y-$ direction
4: end for
5: #pragma omp parallel for
6: for  $j = 1, \dots, N_y; i = 1, \dots, N_x; l = 1, \dots, N_z$  do
7:   Solve the tridiagonal system using LU decomposition
8: end for
9: #pragma omp parallel for
10: for  $l = 1, \dots, N_z$  do
11:   2D inverse DST in  $x-, y-$ direction
12: end for
```

---

We can see that the algorithm is naturally divided into three easily parallelizable parts: forward DST step, the solution of the set of independent tridiagonal systems and the inverse DST transformation step. In all three steps, the OpenMP threads use the different parts of the shared arrays. So the "race conditions" can be easily avoided. The rearranging of the working arrays between three consecutive stages of the algorithm may take significant processing time and must be implemented with careful consideration of array distribution between different types of CPU memory.

In the OpenMP implementation of the developed direct algorithm, a minor complication emerged. An FFTW plan is a necessary function that sets up the calculation of the FFT ([6]) used in DST forward and inverse steps. These plans are not "thread safe" and therefore must be created within a critical region of the parallel section of the code.

Overall, the OpenMP implementation on a single desktop computer with a multicore CPU or on a single multicore node of a cluster demonstrates excellent, near linear scalability. It is perfect for a medium-size grid. We were able to run our test problems with the computational grids up to  $512^3$  grid sizes on a single machine with 16G RAM.

#### 4.2. MPI

As mentioned before, OpenMP provides a very convenient and efficient standard for parallel programming in the shared-memory environment, but for a large enough computational grid, the memory required to allocate the necessary arrays can overrun the RAM available on a single node. The natural solution to a problem is to distribute the working arrays and computational tasks between the nodes of a cluster. But in this case, there is no way for one processor to directly access the address space of another and the need for explicit message passing (MP), i.e. communication between processes becomes obvious. Several specialized languages were developed for this but the standard today is the MPI (Message Passing Interface).

The developed parallel algorithm is well suited for this type of parallelization since the different parallel processes are using different parts of the computational arrays during the course of the program execution. In the developed MPI implementation of the algorithm, the sequential program was modified to run on several nodes allocating only the minimum required memory on

each. This was accomplished by dividing the computational domain as evenly as possible along vertical direction on the DST-transform steps and in the horizontal direction on the independent tridiagonal solvers' step. In turn, this enables the use of much larger computational grids, as the program is no longer limited by the memory of a single node. The usual limitation in this implementation is the significant communication time since MPI processes running in parallel do not have access to the same shared memory. Each process runs the entire program on the assigned (distributed) part of the available memory independently and Communicates with other processes only when explicitly specified by the programmer.

---

**Algorithm 2** MPI 3D Helmholtz Direct Solver

---

```
1: Find  $start_y, start_z, end_y,$  and  $end_z$  using the rank
2: for  $l = start_z, \dots, end_z$  do
3:   2D forward DST in  $x-, y-$ direction
4: end for
5: Scatter the data via MPI to the appropriate process
6: for  $j = start_y, \dots, end_y; i = 1, \dots, N_x;$  do
7:   Solve the tridiagonal system using LU decomposition
8: end for
9: Scatter the data via MPI to the appropriate process
10: for  $l = start_z, \dots, end_z$  do
11:   2D reverse DST in  $x-, y-$ direction
12: end for
```

---

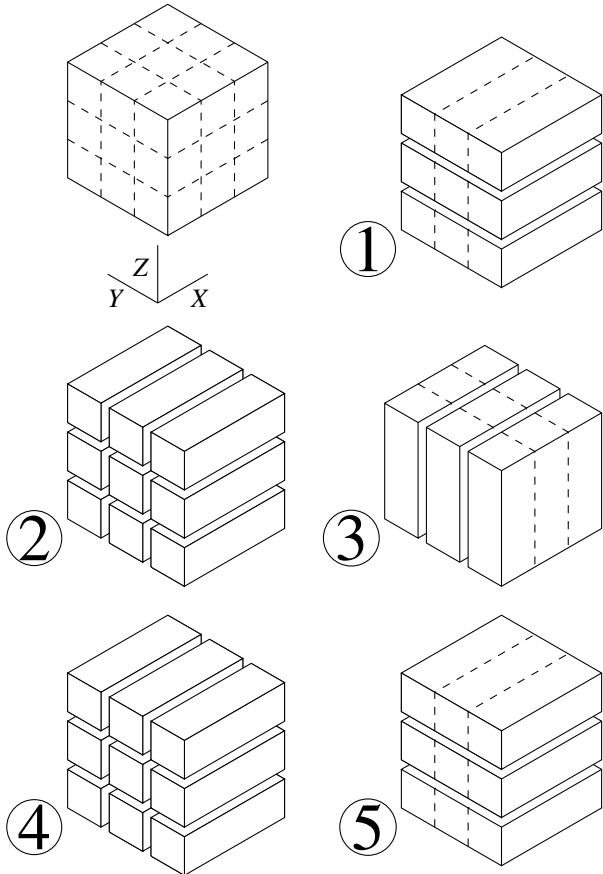
The communication portion of the runtime of the program (wall-time) grows with the number of nodes, so it becomes a major obstacle to the linear scalability of the designed algorithm. Algorithm 2 shows how MPI was used to parallelize the Direct Solver.

The communication between the MPI processes is presented on Figure 2. The key details of the implementation can be considered as follows. If there are  $np$  MPI processes available for parallel execution, then on the 1st step of the parallel algorithm each process performs  $kpz = \lfloor Nz/np \rfloor$  or  $kpz = \lfloor Nz/np \rfloor + 1$  two dimensional sine transforms of the 2D horizontal slices of the 3D array of the right-hand side. After completion of the 1st step, each process will send a part of the 3D array of the transformed data to every other process. The size of the submitted data to another process is  $Nx \times kpy \times kpz$ , where  $kpy = \lfloor Ny/np \rfloor$  or  $kpy = \lfloor Ny/np \rfloor + 1$ . The second step of the process is the solution of the  $Nx \times Ny$  independent tridiagonal linear systems of the size  $Nz \times Nz$ . In this case, the 3D array of the transformed right-hand side is divided along the  $y$ -direction and every process has to solve  $Nx \times kpy$  systems. As a result of the second step the program obtains the transformed solution of the system. Then an individual process sends a portion of this array of the size  $Nx \times kpy \times kpz$  to every other process to set up the last inverse transformation step. This step is executed in the same way as the first forward transformation except for the use of the transformed solution array rather than the array of the right-hand side.

Despite its immense capability, the MPI implementation's performance is limited in this approach. Since the algorithm

uses 2D DST, the program distributes sets of the two-dimensional slices of the 3D working arrays between the processes. This significantly reduces the communication time between the processes in comparison with the transformation step that uses only 1D DST.

Figure 2: Data Transfer between MPI Processes



However, this approach distributes the 2D DST operations in the  $z$  direction of the computational domain in both the forward and inverse transforms. These are the most time expensive steps of the solver. This means that the number of processes which can be used in parallel is bounded by  $N_z$ , the number of grid points in the  $z$ -direction of the computational domain.

#### 4.3. Hybrid

This subsection discusses an approach that combines the advantages of both OpenMP and MPI tools in the presented algorithm. Let's consider a cluster with  $NH$  nodes each with  $KH$  cores. An OpenMP program can only be run on a single node, so only  $KH$  threads can be used for the parallel calculations. As previously mentioned, the number of MPI processes is bounded by  $N_z$  in the MPI implementation. To use the full power of a cluster, that is to utilize all  $NH \times KH$  available cores, it is possible to combine both the OpenMP and MPI tools into a hybrid program. MPI unblocking *Isend* and *Irecv* commands can be

used to transfer data between the nodes where the shared memory is used by OpenMP threads to implement allocated tasks in parallel. This has a clear advantage over using the strictly MPI approach as it will reduce time lost to communication between MPI processes.

In this hybrid case, an MPI process uses an entire node. Then OpenMP allows accesses to every core on the node. As in the case of the MPI implementation, the computational domain needs to be divided along the  $z$ -direction, this number is still bounded by  $N_z$ . However, the hybrid approach uses all available cores on a node via OpenMP threads to parallelize the 2D DST. This is accomplished by using FFTW multi-threading, see ([6]). The implementation of this modified approach is outlined in Algorithm 3.

---

#### Algorithm 3 Hybrid 3D Helmholtz Direct Solver

---

- 1: Create multi-threaded FFTW plan
  - 2: Find  $start_y, start_z, end_y,$  and  $end_z$  using the rank
  - 3: **for**  $l = start_z, \dots, end_z$  **do**
  - 4:   2D forward DST in  $x-, y$ -direction
  - 5: **end for**
  - 6: Scatter the data to the appropriate process
  - 7: **#pragma omp parallel for**
  - 8:   **for**  $j = start_y, \dots, end_y; i = 1, \dots, N_x; l = 1, \dots, N_z$  **do**
  - 9:     Solve the tridiagonal system using LU decomposition
  - 10: **end for**
  - 11: Scatter the data to the appropriate process
  - 12: **for**  $l = start_z, \dots, end_z$  **do**
  - 13:   2D reverse DST in  $x-, y$ -direction
  - 14: **end for**
- 

## 5. Numerical Results

In this section, the results of numerical experiments which demonstrate the quality of the proposed numerical methods are presented. These algorithms were implemented in C programming language and the majority of the numerical experiments were conducted on the "Cori" cluster at Lawrence Berkeley National Laboratories with Haswell nodes. The Haswell nodes contain 32 Intel Xeon Haswell processors with approximately 3.0 GHz clock frequency. For comparison with previously published results we also considered several experiments on a standard iMac desktop with an Intel Core i7, 2.93 GHz processor and 16 Gb of RAM, and a Xeon X5690 server with 144 Gb of RAM.

### 5.1. Sequential implementation of the direct FFT solvers

First, we investigate the efficiency of the developed direct solvers in the case of a 3D test problem and sequential implementation. We choose to demonstrate the quality of the developed direct methods on the test problems recently published in ([7]). The authors of this paper considered the solution of several 3D test problems using iterative multigrid approach. We calculate the solution of the same problems by applying direct algorithms considered in the previous section. In addition, we demonstrate that even the sequential variant of the developed

method is significantly faster than the mentioned iterative solver while implemented on less expensive hardware.

In this problem, the coefficient  $k(z) = a - b \sin(cz)$  with  $a > b > 0$  depends only on one spatial variable, i.e. the developed methods could be used as direct solvers to find an approximate solution to the boundary value problem (1, 2). In our experiments, we use the following measures related to the approximate  $U$  and analytic  $u$  solutions of the problems:

- $L_2$ -res is  $\|AU - F\|_2$ ,
- $L_2$ -err (the relative  $L_2$  error) is  $\|u - U\|_2 / \|u\|_2$ .
- **max-err** is  $\|u - U\|_\infty$ .

In the following numerical experiments the analytic solution

$$u(x, y, z) = \sin(\beta x) \sin(\gamma y) e^{-\frac{k(z)}{c}}, \text{ where } \beta^2 + \gamma^2 = a^2 + b^2$$

is used. We also assume that  $L'_\alpha = 0$  and  $L''_\alpha = \pi$ ,  $\alpha = x, y, z$ . This is the same solution considered in ([7]) up to the notation for the independent variables. Then the right-hand side of (1) is  $f(x, y, z) = -b(2a + c) \sin(cz) e^{-\frac{k(z)}{c}} \sin(\beta x) \sin(\gamma y)$ . We consider the application of the developed direct methods to the solutions obtained by the iterative approach used in [7] on Supermicro cluster consisting of 12 nodes. Each node had two Intel Xeon E5520 quad CPUs running at 2.27 GHz. The two CPUs shared 8 GB of memory. We restrict our consideration to the numerical results with available CPU time and corresponding to the smallest presented in [7] relative  $L_2$  error of 0.001. One can find these results in Tables 2 and 3 in the mentioned paper. For a demonstration of the efficiency of the presented direct solvers we run all test problems on both standard desktop iMac with an Intel Core i7, 2.93 GHz processor and 16 Gb of RAM, and on the Xeon X5690 server.

In the first experiment, we use the following parameters:  $a = 10, b = 9, \gamma = 9$  ( $1 \leq k \leq 19$ ). Table 1 presents a comparison of various solvers: the first two lines the iterative solver used in [7]. Lines from 3 to 8 present results of the second-order direct solver considered in our previous publications ([2], [10]), and fourth and sixth order solvers presented in Section 3 of this paper. Lines 3-5 give results for the iMac PC and lines 6-8 exhibit the results achieved on Xeon X5690 server. The first column represents the hardware used in the numerical experiment. The second and third columns indicate the order of approximation of the solver and the type of the solver (direct or iterative). In the fourth column, the number of grid points needed to reach the indicated relative accuracy ( $L_2$ -err  $< 0.001$ ). The fifth column shows the number of iterations until the convergence of the iterative solver, wherein the case of the direct solvers we put 1. The last column displays the CPU time required for each test run.

Table 1: Comparison of direct and iterative solvers on the first 3-D test problem

SPU	Scheme	Type	$N$	# iter.	Time(s)
SM cl	2	iter.	333	1970	703
SM cl	6	iter.	45	350	1.01
X5690	2	dir.	353	1	15.18
X5690	4	dir.	62	1	0.078
X5690	6	dir.	50	1	.055
iMac i7	2	dir.	353	1	19.8
iMac i7	4	dir.	62	1	.097
iMac i7	6	dir.	50	1	.08

In our experiments, to reach the desired accuracy with the 2nd order approximation scheme we needed to use a  $353^3$  grid, and the direct solver was 46 times faster than the iterative solver. In the case of the sixth order scheme, the direct solver was 5 times faster than the iterative solver. The fastest time was achieved by using the fourth order scheme. We must mention that the CPU time for the sixth order scheme on  $64^3$  grid was 0.07sec and  $L_2$ -err =  $5.2 \cdot 10^{-4}$ . These numbers indicate that due to the optimality condition of the FFT method, sometimes it is advantageous to consider a slightly bigger number of grid points which has more factors of 2 in its prime factorization.

In the next experiment, we consider the same problem with parameters  $a = 80, b = 40, \gamma = 40$  ( $40 \leq k \leq 120$ ) and various values for  $c = 10, 50, 70, 80$ . As in the previous series of numerical experiments, we only consider the solutions of the test problems with the goal of reaching  $L_2$ -err = 0.001. In ([7]), there is no data for second order scheme since it was stated that “the second order scheme could not achieve the error goals with grids of manageable sizes.” We also restrict our consideration to the sixth order direct solvers proposed in this paper. Table 2 displays the results of the numerical experiments for this test problem. The columns of Table 2 are essentially the same as columns of Table 1 except the second column where the values of  $c$  are displayed and the last column where CPU gain factor (T-ratio) in comparison with iterative solver used in ([7]) is indicated.

Table 2: Comparison of direct and iterative solvers on the first 3-D test problem

SPU	c	Scheme	Type	$N$	# iter.	Time
SM clust.	10	6th ord.	iter.	229	200	122
X5690	10	6th ord.	dir.	197	1	1.87
iMac i7	10	6th ord.	dir.	197	1	1.63
SM clust.	50	6th ord.	iter.	266	280	289
X5690	50	6th ord.	dir.	280	1	6.8
iMac i7	50	6th ord.	dir.	280	1	6.9
SM clust.	70	6th ord.	iter.	312	893	642
X5690	70	6th ord.	dir.	326	1	12
iMac i7	70	6th ord.	dir.	326	1	11
SM clust.	80	6th ord.	iter.	> 402	N/A	N/A
X5690	80	6th ord.	dir.	356	1	12
iMac i7	80	6th ord.	dir.	356	1	21

The range of parameters of the last test problems is more closely related to the realistic scenarios of the subsurface scattering problems. We can observe from the table that the direct solvers provide 29-76 times faster alternative than the used iterative approach in ([7]). They also allowed using grids with significantly bigger grid sizes in comparison with the mentioned iterative solver on similar hardware. Table 2 indicates that the iterative solver could not find solutions on the grids greater than  $402^3$ . However, the sixth order direct solver proposed in this paper was successfully applied to the last problem with  $c = 80$  and produce a solution satisfying the desired goal on both iMac and Xeon server. It must be noted that on the  $421^3$  grid, the significant advantage of the Xeon server in RAM becomes crucial for a rapid solution of the problem. It is remarkable that all calculations with direct solvers were conducted on a single Intel Core i7, 2.93 GHz processor with 16 Gb of RAM processor or on Intel Xeon X5690 processor running at 3.47 GHz with 144 Gb of RAM, the frequency of which is similar to only one node in the Supermicro cluster consisting of 12 such nodes on which the iterative solutions were achieved in ([7]). In the majority of our experiments, the sixth order solver allows the achievement of the desired accuracy in less CPU time than the fourth order direct solver, but the possibility of different grid steps in  $x$ -,  $y$ -, and  $z$ -directions makes the fourth order compact scheme an attractive alternative in some situations. Next, we will consider the numerical experiments in which parallel implementation of the developed direct algorithms was investigated.

## 5.2. Scalability of the proposed direct FFT solvers

The results of a sequential implementation of the developed high-resolution compact methods presented in the previous subsection demonstrated higher efficiency of the developed approach in comparison to one of the best, if not the best, iterative methods. However, the advantage of the proposed methodology is natural parallelization of the developed algorithms. This advantage of the considered approach in the case of second and fourth order compact schemes was mentioned in several publications (see e.g. [7]), but the detailed investigation of the scalability of the proposed approach was not considered to the best of our knowledge. This is also the first time the parallel implementation of the sixth order scheme is developed. In the following subsections, we consider the solution of the 3D Helmholtz equation on the grid sizes up to  $4096^3$  and the solution of the 3D convection-diffusion equation to demonstrate the robustness of the presented approach.

### 5.2.1. Helmholtz equation with Constant Coefficient

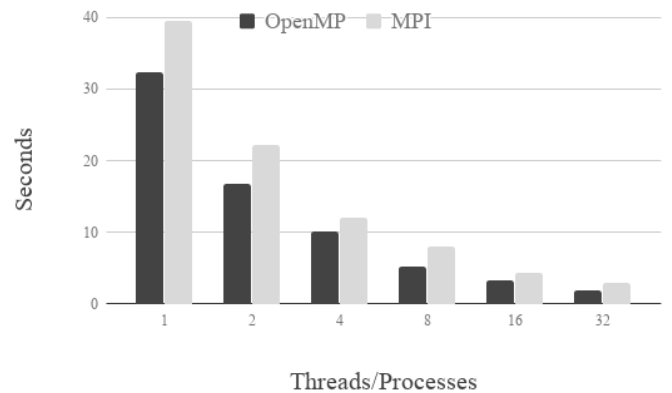
The first parallel experiment used constant coefficient  $k$  with  $a = 20$ ,  $b = 0$ ,  $c = 10$ ,  $\gamma = 16$  and  $\beta = 12$ . In this experiment we used a  $500^3$  grids for the second, fourth and sixth order of approximation compact schemes. The Table 3 represent the implementation of the direct compact solvers in OpenMP environment on the standard 8 cores desktop. We can see that the wall-time of parallel implementation of every compact scheme demonstrates linear scalability. In all three cases we have close to a 16 times decrease in wall time of the considered OpenMP implementation of the developed algorithms.

Table 3: Desktop solution time for OpenMP

order\# of threads	1	2	4
2 <sup>nd</sup>	36.81 sec	18.77 sec	9.62 sec
4 <sup>th</sup>	36.02 sec	16.71 sec	9.96 sec
6 <sup>th</sup>	46.45 sec	17.62 sec	9.51 sec

Figure 3 shows the computation time in seconds of the Direct Solver. The results come from the sixth order scheme with a grid size of  $500^3$ . In order to compare the performance of OpenMP and MPI directly, both were run on a single node on Cori.

Figure 3: Computation Time OpenMP vs MPI Restricted to a single node



These results are desirable and expected. As the number of processing units is doubled the computation time is reduced by nearly half while approaching the bottleneck. It is expected to see this curve in the graph as the benefit of splitting the tasks across multiple processing units decreases when there are fewer required computations. It is also expected to see a better performance by OpenMP on a single node since MPI requires the processes to communicate with each other.

### 5.2.2. Helmholtz equation with Variable Coefficient

Next, we consider the performance of the proposed parallel algorithms in the case of nonconstant coefficient  $k^2(z)$ . We consider the test problem with  $a = 10$ ,  $b = 9$ ,  $c = 10$ ,  $\gamma = 9$  and  $\beta = 10$ . Tables 4, 5 and 6 demonstrate the convergence of the second, fourth and sixth order implementations respectively.

Table 4: Second Order Convergence

	Second Order		
	max-err	$L_2$ -err	$L_2$ -res
$125^3$	5.7570466e-03	6.4986713e-03	4.7269292e-13
$250^3$	1.4853854e-03	1.6510028e-03	2.5846930e-12
$500^3$	3.7448165e-04	4.1516358e-04	6.5883688e-12



Table 5: Fourth Order Convergence

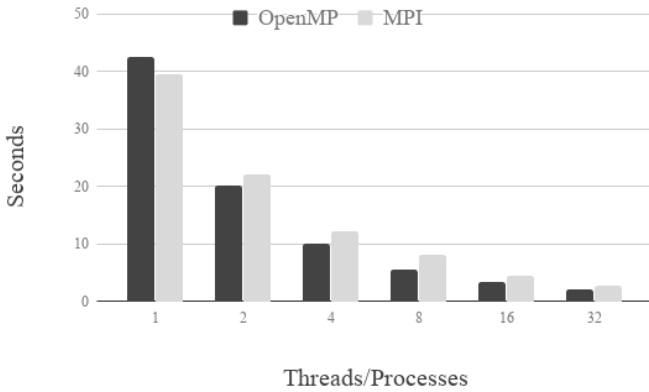
	Fourth Order		
	max-err	$L_2$ -err	$L_2$ -res
$125^3$	3.4493268e-05	3.5925614e-05	3.6301725e-13
$250^3$	2.1782070e-06	2.2582699e-06	1.9857221e-12
$500^3$	1.3726414e-07	1.4187594e-07	5.0832056e-12

Table 6: Sixth Order Convergence

	Sixth Order		
	max-err	$L_2$ -err	$L_2$ -res
$125^3$	2.1875397e-06	1.9909214e-06	3.1581209e-13
$250^3$	3.4942928e-08	3.1643311e-08	2.0541112e-12
$500^3$	5.5211108e-10	4.9939925e-10	5.2147803e-12

As desired, these errors reduce with their respective order of approximation when the grid size is doubled in each direction. This experiment was also run in order to compare to the results found in [7]. Figure 4 shows excellent acceleration nearly identical to Figure 3. These results are run with a grid size of  $500^3$  already surpassing the maximum grid size achieved in [7], i.e.  $402^3$ .

Figure 4: Computation Time OpenMP vs MPI Restricted to a single node

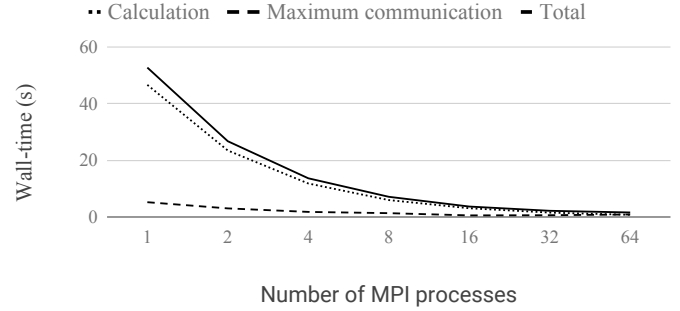


The limitations of OpenMP were observed in the attempt to run an experiment with the grid size of  $1000^3$ . A single node on Cori and other machines tested were unable to run this test due to lack of memory. Next, the experiment was repeated with MPI on one, two and four nodes. The first to successfully run the program was with four nodes. This demonstrates the power of the MPI implementation.

A test was conducted to study the strength and limitation of MPI implementation in this algorithm. The computation and communication time is recorded as the number of MPI processes increased. Here computation time refers to the time taken for the MPI processes to complete the forward and reverse 2D DST and tridiagonal solver. The communication time

measures the longest time taken for the MPI processes to scatter the data to the appropriate processes and assigning data to a local array. This test is run on a grid size of  $512^3$  and Figure 5 shows the results.

Figure 5: Computation, Communication and Calculation Time for MPI On Cori



The results are desirable and expected. As the number of MPI processes is doubled the computation time is reduced by nearly half. On the other hand, communication has little changes across one to eight MPI processes. Nonetheless, the communication time is reduced by half when the number of MPI processes increase from 8 to 16. Beyond 16 MPI processes, the communication time is seen to increase. This suggests that the setup time (overhead) has increased. At 64 MPI processes, the communication time has exceeded the computation time in this particular test. This test demonstrated the limitation of the MPI implementation due to communication time.

To present the performance of the hybrid implementation the number of MPI processes, i.e. nodes, were doubled. Additionally, the number of OpenMP threads were doubled. Table 7 shows the computation times in seconds for each run on the same grid size. Here the number of OpenMP threads change horizontally and the MPI processes change vertically.

Table 7: Hybrid Implementation

n\t	1	2	4	8	16	32
1	39.61	24.56	15.04	10.78	8.88	8.07
2	19.90	11.90	7.19	4.97	4.00	3.44
4	10.31	6.11	3.66	2.60	2.28	1.90
8	5.30	3.34	2.09	1.52	1.30	1.22
16	2.42	1.48	0.85	0.55	0.47	0.41
32	1.81	1.35	1.06	0.86	0.77	0.86

The performance with strictly MPI, i.e. one thread, performs as expected. However, in the case of restricting hybrid to one node while increasing the number of OpenMP threads the performance is not as good as the strictly OpenMP implementation. This is likely due to the use of OpenMP to parallelize 2D DST. A parallel region is created every time the algorithm performs a 2D DST. This increases the overhead time hence reducing the overall performance of OpenMP. However, hybrid

implementation shows desirable results. The drastic improvement was seen when increasing the number of nodes from 8 to 16 could be explained by the improvement in communication time as seen in Figure 5.

Further experiments were run to compare the performance of the MPI and hybrid implementations. This was done to test the theory that reducing the number of MPI processes while maintaining the number of physical processors utilized will improve the computation time over MPI. Tables 8 and 9 give these results.

Table 8: Large Grid MPI

Grid	Nodes	MPI processes	Seconds
512 <sup>3</sup>	1	32	2.830525
1024 <sup>3</sup>	4	128	8.759851
2048 <sup>3</sup>	32	1024	40.465395
4096 <sup>3</sup>	256	4096	445.803343

Table 9: Large Grid Hybrid

Grid	Nodes	Processors	Seconds
512 <sup>3</sup>	1	32	7.793963
1024 <sup>3</sup>	4	128	16.911352
2048 <sup>3</sup>	32	1024	19.417831
4096 <sup>3</sup>	256	8192	27.522366

While running this algorithm on a smaller grid size with less MPI processes, the MPI implementation performed much better than the hybrid implementation. This is likely due to the overhead required by OpenMP. When working with a grid size of 2048<sup>3</sup> the communication time becomes a bottleneck in the MPI implementation since a total of 1024 MPI processes are required. In the hybrid implementation, only 32 MPI processes are needed for the same grid size. This significantly reduces the communication time. The grid size 4096<sup>3</sup> also demonstrates another limitation of MPI implementation. As mentioned in Section 4.2 the MPI implementation is only able to utilize at most 4096 processes. The hybrid implementation, however, is capable of utilizing as many MPI processes as processors available on the machine. Therefore, the Hybrid implementation outperforms the strictly MPI program by 16 times.

### 5.2.3. Convection-diffusion equation.

This section presents the application of the developed direct parallel algorithms to the convection-diffusion equation (8). Since this is simply an illustration of the diversity of applications of the proposed method, we restrict the consideration to the OpenMP implementation. The test problem under consideration can be presented as

$$\nabla^2 u + \gamma \frac{\partial u}{\partial z} = 0, \quad \text{in } \Omega, \quad (10)$$

where  $\gamma = -100$  and on  $\Omega = [0, \sqrt{2}] \times [0, \sqrt{2}] \times [0, 1]$ . With boundary conditions:  $u(x, y, 0) = \sin\left(\frac{\pi x}{\sqrt{2}}\right) \sin\left(\frac{\pi y}{\sqrt{2}}\right)$ ,

$u(0, y, z) = u(\sqrt{2}, y, z) = u(x, 0, z) = u(x, \sqrt{2}, z) = 0$ ,  
 $u(x, y, 1) = 2 \sin\left(\frac{\pi x}{\sqrt{2}}\right) \sin\left(\frac{\pi y}{\sqrt{2}}\right)$ , where  $0 \leq x, y \leq \sqrt{2}$  and  $0 \leq z \leq 1$ . The analytic solution of the problem is given by

$$u = \sin\left(\frac{\pi x}{\sqrt{2}}\right) \sin\left(\frac{\pi y}{\sqrt{2}}\right) e^{-\mathcal{R}z/2} \frac{2e^{\mathcal{R}/2} \sinh(\sigma z) + \sinh(\sigma(1-z))}{\sinh \sigma}$$

where  $\sigma = \sqrt{\pi^2 + \mathcal{R}^2/4}$ . The convergence of the approximate solution to the analytic solution on a sequence of grids is presented in the following table

Table 10: Maximum Error

Grid size $k$	$\ u - U\ _\infty$
64 <sup>3</sup>	3.2612907e-03
128 <sup>3</sup>	2.0579387e-04
256 <sup>3</sup>	1.2939970e-05
512 <sup>3</sup>	8.1975702e-07

The next table gives the results of the parallel calculations on a standard laptop with 8 cores. The number of OpenMP threads in this test varies from 1 to 8. The table presents the "wall time" required by the direct solver for two grid sizes 256<sup>3</sup> and 512<sup>3</sup>. We can see that the proposed parallel algorithm gives almost four times speed up in comparison with a sequential implementation. This test shows that this approach can be used to construct an efficient preconditioner in a variety of important applications.

Table 11: Seconds to Compute

OpenMP Threads	256 <sup>3</sup>	512 <sup>3</sup>
1	7.858606	40.0879
2	4.557636	24.553443
4	2.666061	15.109893
8	1.828526	10.878381

## 6. Conclusion

In this paper, a direct parallel generalized FFT type algorithm was developed for a class of compact numerical approximations on a rectangular grid. The target applications of high-order compact approximation of 3D Helmholtz and convection-diffusion equations were considered on a sequence of grids. The developed algorithms represent highly accurate and scalable methods for the solution of the considered problems. The results demonstrated the efficiency of the OpenMP, MPI and Hybrid implementations of the proposed parallel algorithms. This includes the vast improvement in computation time and the ability to apply these methods to other schemes with similar 3D stencils.

## 7. Acknowledgements

The authors gratefully acknowledge the financial support from the Sustainable Horizons Institute and Lawrence Berkeley

National Laboratory(LBNL) in the form of the summer fellowships for all three authors at LBNL during summer 2018.

## References

### References

- [1] Y.Zhuang, X.-H.Sun, A high-order fast direct solver for singular poisson equations, *J. Comput. Phys.* 171 (2001) 79–94.
- [2] Y. Gryazin, Preconditioned krylov subspace methods for sixth order compact approximations of the helmholtz equation, *ISRN Computational Mathematics*, (2014) 1–15, doi:10.1155/2014/745849.
- [3] Y. A. Gryazin, High order approximation compact schemes for forward subsurface scattering problems, in: *Proceedings of the SPIE 9077, Radar Sensor Technology XVIII Conference*, 2014, pp. 1–9. doi:10.1117/12.2050189.
- [4] H. Elman, D. O’Leary, Efficient iterative solution of the three-dimensional helmholtz equation, *J. Comput. Phys.* 142 (1998) 163–181.
- [5] H. Elman, D. O’Leary, Eigenanalysis of some preconditioned helmholtz problems, *Numer. Math.* 83 (1999) 231–257.
- [6] Frigo, M., Johnson, S., *FFTW Manual*, Massachusetts Institute of Technology (2003).
- [7] E. Turkel, D. Gordon, R. Gordon, S. Tsynkov, Compact 2d and 3d sixth order schemes for the helmholtz equation with variable wave number, *Journal of Computational Physics* (2012) 272–287.
- [8] S. Lele, Compact finite difference schemes with spectral-like resolution, *Journal of Computational Physics* 103 (1992) 16–42.
- [9] D. D. J. Kalita, A. Dass, A transformation-free hoc scheme for steady convection-diffusion on non-uniform grids, *Int. J. Numer. Meth. Fluids* (2004) 33–53.
- [10] Y. Gryazin, M. Klibanov, T. Lucas, Gmres computation of high frequency electrical field propagation in land mine detection, *J. Comput. Phys.* 158 (2000) 98–115.